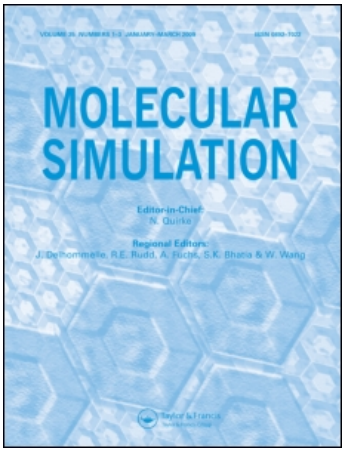

Molecular Simulation
Publication details, including instructions for authors and subscription information:
http://www.informaworld.com/smpp/title~content=t713644482

Molecular dynamics simulations of submonolayer hexane and pentane films on graphite

M. W. Roth[a]; M. Kaspar[a]; Carlos Wexler[b]; L. Firlej[c]; B. Kuchta[d]
[a] Department of Physics, University of Northern Iowa, Cedar Falls, IA, USA [b] Department of Physics and Astronomy, University of Missouri, Columbia, MO, USA [c] LCVN, Université Montpellier 2, Montpellier, France [d] Laboratoire Chimie Provence, Université de Provence, Marseille, France

First published on: 26 November 2009

To cite this Article Roth, M. W. , Kaspar, M. , Wexler, Carlos , Firlej, L. and Kuchta, B.(2010) 'Molecular dynamics simulations of submonolayer hexane and pentane films on graphite', Molecular Simulation, 36: 4, 326 — 333, First published on: 26 November 2009 (iFirst)
To link to this Article: DOI: 10.1080/08927020903437839
URL: http://dx.doi.org/10.1080/08927020903437839

Molecular Simulation
Vol. 36, No. 4, April 2010, 326–333

Taylor & Francis
Taylor & Francis Group

Molecular dynamics simulations of submonolayer hexane and pentane films on graphite

M.W. Roth[a]*, M. Kaspar[a], Carlos Wexler[b], L. Firlej[c] and B. Kuchta[d]

[a]*Department of Physics, University of Northern Iowa, Cedar Falls, IA 50614, USA;* [b]*Department of Physics and Astronomy, University of Missouri, Columbia, MO 65211, USA;* [c]*LCVN, Université Montpellier 2, 34095 Montpellier, France;* [d]*Laboratoire Chimie Provence, Université de Provence, 13396 Marseille, France*

(*Received 23 July 2009; final version received 25 October 2009*)

We present results of molecular dynamics computer simulations of hexane (C_6H_{14} or C6) and pentane (C_5H_{12} or C5) adlayers physisorbed onto a graphite substrate, for various submonolayer coverages. The hexane and pentane molecules incorporate explicit hydrogens and the graphite is modelled as a six-layer all-atom structure. Even though C6 and C5 have different structures at monolayer completion, both systems generally behave similarly in the submonolayer regime and results are in reasonable agreement with experiment for both systems. Specifically, there are four distinct topological regimes involving empty space: at densities closest to full coverage, there are large domains with individual vacancies, then with decreasing density, large vacancy patches appear first, followed by the formation of connected networks of smaller domains with multiple orientations that ultimately separate into individual patches. The energetics and melting behaviour of all systems are readily understood within the framework of the topology presented at various densities.

Keywords: simulations; hexane; pentane; submonolayer; graphite

1. Introduction

Understanding the behaviour of carbon compounds – the compounds of life and fossil fuels among other things – is part and parcel to our ability to better control, care for and utilise our environment. Hydrocarbons are molecules that contain only hydrogen and carbon, and of them alkanes (with the general chemical formula C_nH_{2n+2}) are probably the most widely used – in heating, lighting, transportation, machinery, detergents, lubrication, refining, adhesives and many others. It is this ubiquitous usefulness that motivates us to choose them to study. As a chemical family, they are a nice compromise of simplicity (as far as organic molecules go) and complexity (their internal degrees of freedom can affect the overall system behaviour). In their conventional bulk (three-dimensional) regime, many physical properties of alkanes can be fairly precisely related to their molecular structures. However, they behave in interesting and counter-intuitive ways while physisorbed onto surfaces. It is because of the modification of system interactions through a strong substrate–adatom interaction that the molecules interact more strongly with each other than they do in the bulk. As a result, such quasi-two-dimensional systems exhibit a rich landscape of behaviour not realised in the system's corresponding bulk state.

Short alkanes ($n < 12$) adsorbed onto a graphite substrate behave markedly different when n is odd and even. At monolayer coverage, odd alkanes form a low-temperature solid rectangular-centred (RC) phase that is commensurate for $n = 7$ and 9 but not for $n = 5$ [1–6]. X-ray and neutron diffraction studies of pentane and heptane on graphite at a coverage of 1.01 monolayers concluded that combinations of rotated RC and herringbone phases are present [2].

For pentane near monolayer completion, a sharp melting transition has been found at *c*.99–105 K [3–6]. Furthermore, it appears that the solid monolayer does not coexist with a bulk fluid phase, but melts very near to the bulk melting temperature of pentane [3]. The issue of solid–fluid coexistence is important and in fact can help validate the thermodynamic accuracy of molecular simulations. With that in mind, the most recent study on pentane concluded that melting for 1.01 monolayers takes place from an RC solid at $T_m = 99$ K and presents a coexistence of dense clusters with the fluid through a temperature range of about 30 K above melting [6]. A similar effect has been observed for C6 on graphite but over a shorter temperature range after melting [7–12].

Hexane on graphite was first studied by Krim et al. [7] using both the low-energy electron diffraction and the neutron diffraction. For submonolayer coverage ($\rho \sim 0.93$) and low temperature, a uniaxial incommensurate (UI) herringbone phase was observed, melting at about $T = 151$ K in a first-order transition; however, a determination of the molecular orientations was not possible. As the coverage is increased, the UI phase evolves continuously into a $2 \times 4\sqrt{3}$ commensurate structure at completion. More recently, Taub and co-workers [7–12] completed extensive neutron and X-ray diffraction studies of hexane

*Corresponding author. Email: rothm@uni.edu

ISSN 0892-7022 print/ISSN 1029-0435 online

DOI: 10.1080/08927020903437839
http://www.informaworld.com

on graphite for submonolayer [8,9], monolayer [10–12] and multilayer [7] coverages. Their findings indicate that, at low temperatures, a complete monolayer forms a commensurate herringbone structure that evolves with increasing temperature into an RC solid–liquid coexistence region by *c.*150 K and melts at around 175 K [7]. For submonolayer coverages, the authors proposed a structure corresponding to a UI phase comprising commensurate regions separated by low-density fluid-filled domain wall [8].

Initial computational work on C6/gr has been done at monolayer completion using united-atom (UA) approximation [10–17] or fully atomistic (explicit hydrogen) models [18–21]. Simulations with the hydrogens explicitly included, and with the molecular flexibility correctly accounted for with a CHARMM22 non-bond scaling factor (SF), accurately reproduce the experimental features of the C6/gr system [21]. Generally, simulations of C6 on graphite show the three distinct phases discussed earlier – the solid, nematic mesophase and the fluid – without much contribution from molecular flexibility. Recent work suggested that, at completion (defined as the largest density giving zero spreading pressure), the system presents the solid and liquid, with the nematic mesophase being absent [21].

In contrast to the wealth of reported short-alkane simulations near monolayer completion, submonolayer alkane systems have not been widely modelled. The purpose of the present work is to better understand the statics and dynamics of short-alkane submonolayer films and relate their behaviour to topological features of the adlayer. We compare and contrast the behaviour of two alkanes (C5 and C6) close in length but of different parity, and therefore complement a recent study of the dynamic behaviour of domains in C6 on graphite near completion [17,21].

2. Simulation tools and set-up

We utilise the NAMD code [22] – a parallelised MD simulation package which has been carefully developed and validated for different systems such as nucleic acids [23] and lipid bilayers (available at http://www.wwpdb.org/, [24]). The optimisations and parallelisation of NAMD permitted us to offset the extra computational time cost of the hydrogen inclusion by running these in parallel clusters of off-the-shelf computers. In addition, we have written pre- and post-processors in order to generate system-specific input files and to reduce the resulting output files, respectively.

All simulations in this study are in the constant molecule number, coverage and temperature ensemble (N, ρ, T). The hexane and pentane molecule definitions are obtained from the Brookhaven Protein Data Bank (available at http://www.wwpdb.org/). Because NAMD currently does not include an analytical expression for adatom–substrate interactions (such as Steele's expression [25]), the substrate has been modelled as an all-atom system, built up from six identical graphene sheets stacked in the (*-A-B-A-B-*) pattern in the *z*-direction. Appropriate substrate indices n_x and n_y are given in Table 1, and the corresponding substrate dimensions are given by multiplying the indices with the graphite unit-cell dimensions $a_x = 4.26$ Å and $a_y = 2.46$ Å. Table 1 also shows adlayer molecule numbers and densities; the densities are calculated based on the area per molecule at experimentally determined completion (~ 42 Å^2 per molecule for C6 [7] and ~ 37 Å^2 per molecule for C5 [6]) and are quoted here as estimates of mean density of the adlayer only. Periodic boundary conditions are used in the (x, y) plane and free boundary conditions are applied in the vertical direction (z). To maintain a constant temperature, velocity rescaling is utilised. The integrator's time step for all simulations is 1 fs. Each simulation sequence at a given (ρ, T) was started from the end point of a preceding one, subsequently equilibrated for 3 ns and then ran for the next 5 ns in production, where thermal averages were calculated. For the first simulations in a given sequence, the system was also allowed to relax for 0.1 ns at low temperature from the initial configuration so that it could achieve a given lattice topology before the equilibration/production runs.

Table 1. Integer dimension values (n_x *and* n_y), molecule number N, densities ρ and melting temperatures T_m for various C6 and C5 simulations.

Species	n_x	n_y	N	ρ (ML)	T_m (K)
C6	32	56	416	0.929	170
C6	34	56	416	0.874	145
C6	36	56	416	0.826	143
C6	38	56	416	0.782	140
C6	39	67	416	0.637	140
C6	44	78	416	0.485	135
C6	50	80	416	0.416	130
C6	64	112	416	0.232	125
C5	30	60	480	0.933	100
C5	35	60	480	0.8	100
C5	42	79	480	0.506	95
C5	60	112	480	0.267	90

Notes: Here, the densities are calculated based on area per molecule in the previous work for C6 and C5 [6,7] and represent average characteristics of the system. ML, monolayer.

2.1 Interaction potentials

All particle–particle interactions in the simulations presented here are in the standard CHARMM22 format [26]. There are three types of internal (bonded) interactions between atoms within the same molecule and two types of non-bond interactions between adsorbate atom pairs as well as adsorbate atoms and carbons in the graphene sheets composing the substrate. In addition, there

Table 2. Expressions for the types of interaction potentials used in the C6/gr simulations in this work.

Interaction potential	Type	Formula
Bond stretching	Intra; bonded; two-body	$u_{\text{stretch}} = k(l - l_0)^2$
Bond angle bending	Intra; bonded; three-body	$u_{\text{bend}}(\theta) = k_\theta(\theta - \theta_0)^2$
Dihedral torsion	Intra; bonded; four-body	$u_{\text{dihed}} = k_{\text{d}}\{1+\cos(n\phi_{\text{d}} - \delta)\}$
van der Waals (modified Lennard-Jones)	Inter; non-bond; two-body	$u_{\text{LJ}}(r_{ij}) = \varepsilon_{ij}[(r_0/r_{ij})^{12} - 2(r_0/r_{ij})^6]$
Coulomb (electrostatic)	Inter; non-bond; two-body	$u_{\text{C}} = kq_iq_j/r_{ij}$
Scaled non-bond (Coulomb and van der Waals)	Intra; non-bond	Excluded for 1–3 pairs; scaled for 1–4 pairs and fully included for 1–5 and more distant pairs

Notes: Interactions between atoms on the same molecule are classified as 'intra' and those between atoms on different molecules or adatom–substrate interactions are tagged as 'inter'.

are scaled non-bond interactions between atoms of the same molecule. All interactions used in the simulations presented here are summarised in Table 2; more details as well as potential parameters are given elsewhere [18–20,27].

Molecular flexibility is a central feature in alkane simulations and must be accurately represented. This flexibility is, in part, determined by the correct accounting of *intramolecular* van der Waals and Coulomb interactions. In CHARMM22, such non-bonded interactions for 1–3 pairs (first through third neighbours on the same molecule) are not included, those for 1–5 and beyond are fully included and the 1–4 interactions are reduced by a 'SF'. A previous study [20] on a variety of alkanes on graphite determined that SF $\cong$ 0.8 is the correct value for hexane, and is used in this paper (previously, ad hoc values SF $\cong$ 0.5 were generically used, even though this value has no justification and leads to incorrect melting temperatures [20]). In the case of pentane, simulations near monolayer completion were insensitive to the variations in molecular flexibility through changing values for SF.

3. Results and discussion

Both the C6 and C5 simulations were run at densities well below monolayer completion, and the resulting structures (an RC-oriented lattice for C5 and a commensurate herringbone for C6) are in good agreement with experiment [1–12]. Figures 1 and 2 show final snapshot configurations for low-temperature structures of C6 and C5 layers, respectively, for all densities studied here. Generally, there are four distinct topological regimes that are realised in different density ranges. At the highest densities examined in this work ($\rho \sim 0.9$), the low-temperature solids present small mobile vacancies and fairly large domains. As density decreases, $0.9 > \rho > 0.8$, the vacancies coalesce into larger vacancy patches and the system sacrifices its orientational order in favour of a larger number of smaller domains having different orientations. Further decrease in density, $0.8 > \rho > 0.4$, transforms the adlayer into a connected network of molecules, as domain size shrinks and their number increases. When density becomes low enough, $\rho < 0.4$, the system cannot support the connected network anymore

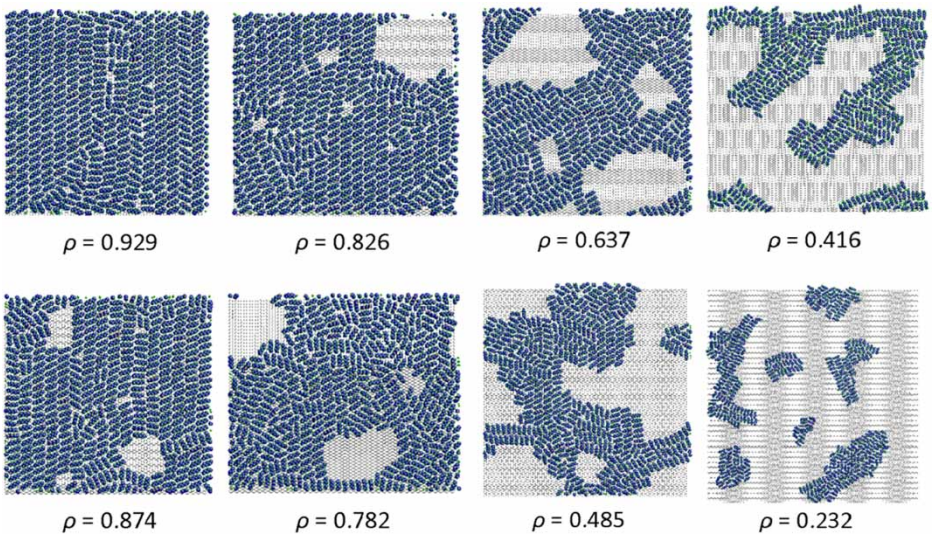

Figure 1. Final snapshot configurations for the low-temperature C6 solid ($T = 100$ K) at various densities that correspond to those given in Table 1.

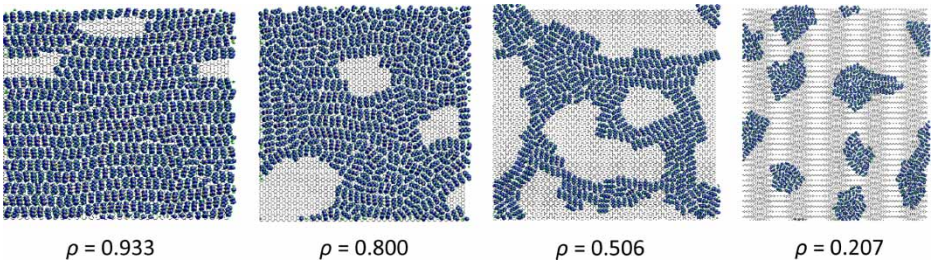

Figure 2. Final snapshot configurations for the low-temperature C5 solid ($T = 80$ K) at various densities that correspond to those given in Table 1.

and breaks into patches. This behaviour is in accordance with the experimental observations [1–12]. In C6, a UI phase exists for near-monolayer densities [8] and has been studied in the UA [17] and all-atom [19] approximations. However, the densities analysed in the present study are below those where such a phase should be stable.

The domain behaviour has been further analysed by examining the azimuthal angle distribution of the long axis of the molecules for both species (Figure 3). At monolayer completion [19], the C6 monolayer presents a herringbone structure characterised by the appearance of two peaks separated by $\sim 120^\circ$ in azimuthal angle distribution for $\rho = 1$. When density is slightly decreased, the UI herringbone phase [19], with slightly relaxed orientational order, appears. Then, as layer density decreases further, the large domains with predominantly herringbone orientation disappear and the loss of overall order in favour of multiply-oriented smaller domains following the orientation of the graphite underlayer is clearly visible. The behaviour for C5 is similar, although the structure disorients with decreasing density from the RC stacked one (characterised by two peaks separated by $\sim 180^\circ$ for $\rho = 0.9333$).

When the density of adlayers decreases, significant differences between C6 and C5 behaviour appear (Figure 4). For C6, the first neighbour spacing increases

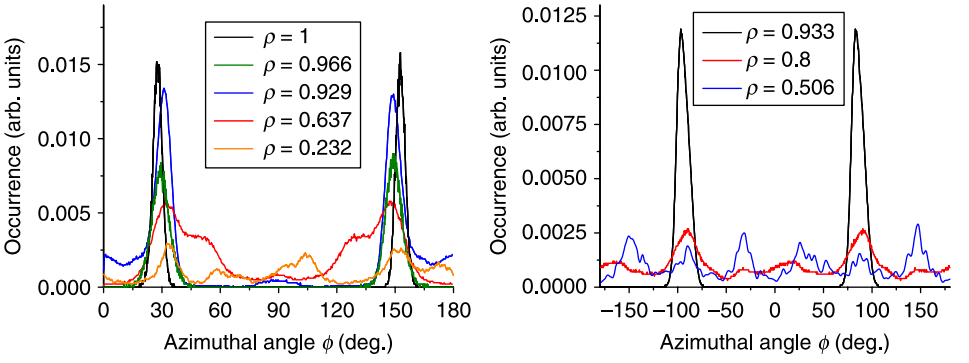

Figure 3. Azimuthal angle probability distributions at various densities in the low-temperature solid for C6 (left panel) and C5 (right panel). (Colour online).

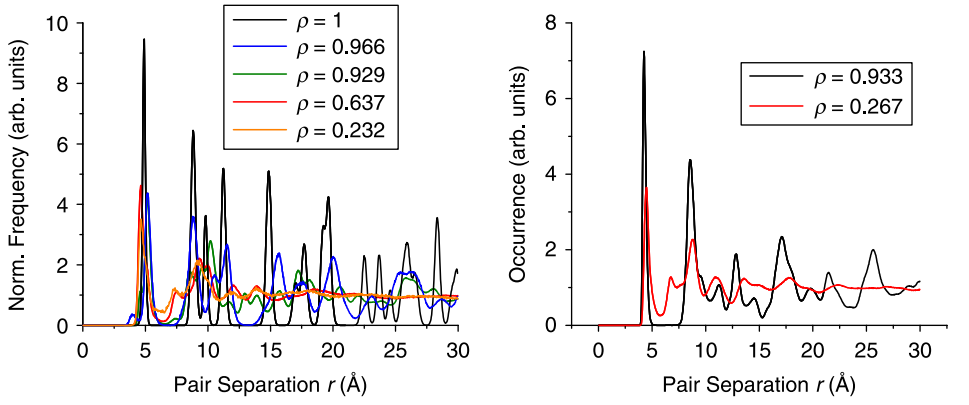

Figure 4. Pair correlation function $g(r)$ in the low-temperature solid for C6 (left panel) and C5 (right panel). (Colour online).

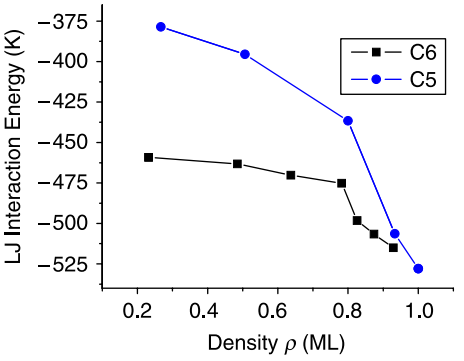

Figure 5. LJ interaction energy per particle for C6 (squares) and C5 (circles) in the low-temperature solid. The densities are normalised to full coverage as described earlier. (Colour online).

with decreasing density throughout the UI phase and then decreases when the density is too low to support the UI phase and vacancies appear. For C5, the first neighbour spacing C5 increases when vacancies are formed. The presence of a greater number of domains with multiple orientations is confirmed by the increasing fluid-like character in the long-distance tail for the pair correlation function, $g(r)$, in both systems.

The transitions between various topological regimes are governed by energy considerations. Figure 5 shows the behaviour of the thermal average of the non-bonded Lennard-Jones (LJ) intermolecular interaction in both systems. Along with the snapshots shown, the steep parts of the curves reveal that the formation of individual vacancies and even small vacancy patches cost the systems a considerable amount of energy. For both systems, there is a density ($c.0.8$) below which both systems transition to lower densities by reorganising the shape of domains but not creating more vacancies. As the system transitions from the connected networks to individual patches, the system is still reorganising but not creating vacancies, and so the LJ interactions do not show such a signature.

Figure 6 shows the order parameters OP_{nem}, OP_2 and Φ_6 as functions of density in the low-temperature solid.

The three order parameters are defined as

$$OP_{nem} = \left| \frac{1}{N_m} \sum_{i=1}^{N_m} \cos 2(\varphi_i - \varphi_{dir}) \right|, \quad (1)$$

$$OP_2 = \left| \frac{1}{N_m} \sum_{i=1}^{N_m} \cos 2\varphi_i \right| \quad (2)$$

and

$$\Phi_6 = \left| \frac{1}{N_b} \sum_{k=1}^{N_b} \exp(\text{in } \theta_k) \right|. \quad (3)$$

Details of the order parameters are given elsewhere [14–17,27], but a brief discussion here is warranted. OP_{nem} is the nematic order parameter and monitors ϕ_i, the angle that the axis of the lowest principal moment of inertia of molecule i makes with the x-axis in the simulation box. It gives an indication of the amount and size of stacked domains present having an overall (or average) director oriented at an angle ϕ_{dir} [16]. OP_2 monitors the same molecular orientation angle and is a measure of twofold molecular orientational order, taking on a limiting value of 1 when the long axes of all molecules in the system are aligned in the direction of the x-axis [27]. OP_{nem} and OP_2 are useful in tandem because the former deals with orientation relative to an average *overlayer* director, while the latter quantifies orientation relative to the substrate. In principle, the two parameters could show different behaviours related to the system's domain structure and dynamics, but in this paper they show similar signatures. Finally, Φ_6 is the hexagonal order parameter and quantifies the amount of sixfold bond-orientational order the system has, taking on a limiting value of 1 for a perfectly triangular or hexagonal lattice [27]. Inspection of Figure 6 confirms that the formation of vacancies and small isolated vacancy patches takes place in concert with structural reordering until a density of about 0.8, below which vacancy formation is pre-empted

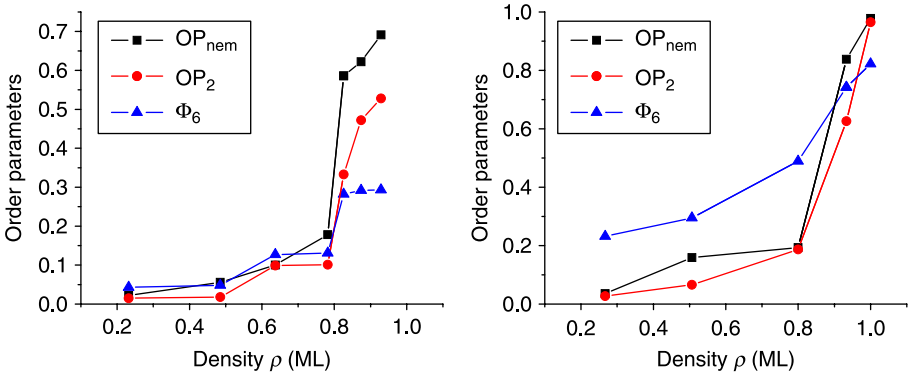

Figure 6. Order parameters OP_{nem} (squares), OP_2 (circles) and Φ_6 (triangles) as functions of density in the low-temperature solid for C6 (left panel) and C5 (right panel). (Colour online).

by reshaping of the exterior of the system with changing density. The picture is very similar to that for C5.

Normally, various order parameters are used to determine the melting transition temperature. Most of them are not useful in characterisation of submonolayer systems as they may have very low values even in the low-temperature solid, as illustrated in Figure 6. Since the pair correlation function $g(r)$ can differentiate between solid and liquid for first and second neighbour shells even at the lowest densities studied here, it is employed as a universal indicator of melting. Table 1 shows melting temperatures T_m for C6 and C5 for various densities.

The systems' melting may be characterised in relation to its topological and domain properties. Figure 7 shows representative snapshots for C5 in the four density regimes for the solid, near melting and the liquid phase; the behaviour of C6 is very similar. For both systems, T_m drops dramatically with increasing density in the region where small vacancies and small isolated vacancy patches proliferate. In this region, melting results in domain expansion which causes the vacancies to be filled in. As more vacancy space is accessible (lower system density), the system has more room to expand into and T_m decreases. When the vacancy patches are large enough, the system does not completely fill them in when it melts; therefore, T_m becomes insensitive to density changes. Similarly, for all densities $\rho < c.0.8$, T_m remains density independent because the edge molecules can diffuse and are not constrained by the area they are expanding into (they do not fill up the entire space upon melting). In the lowest density regime, the melting temperature becomes again density sensitive because the size of molecular clusters is small and the ratios of the number of molecules on patch boundary to those in the patch interior are large.

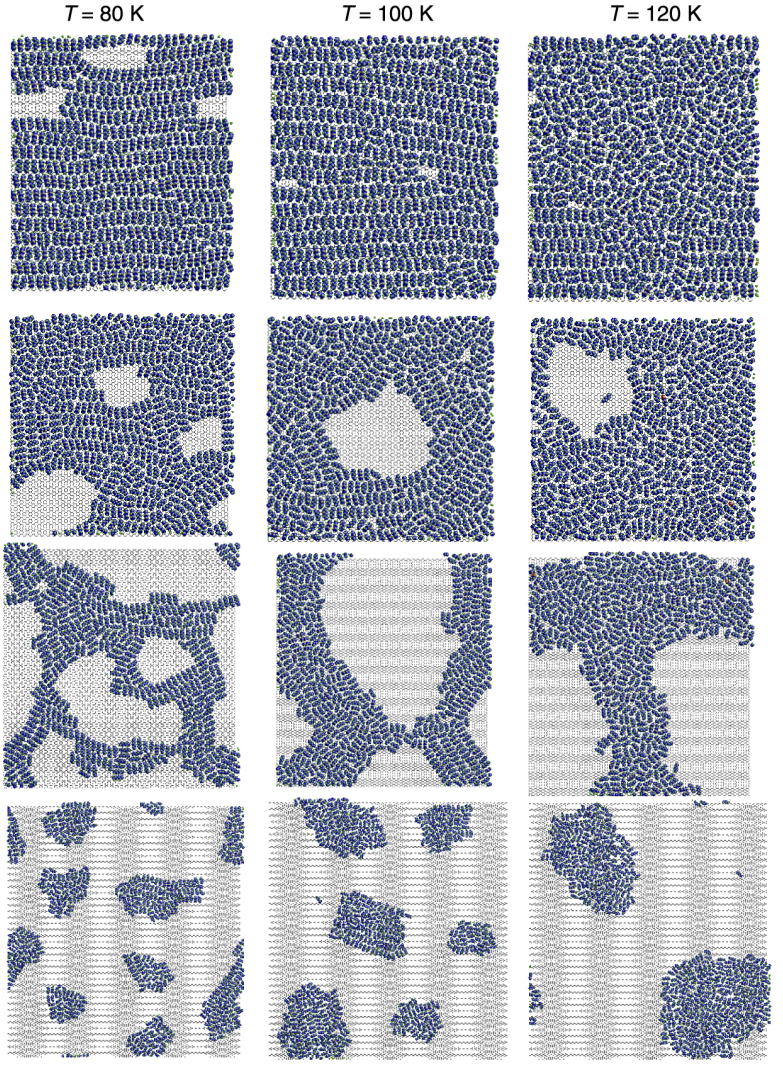

Figure 7. Final configuration snapshots of C5 in the solid ($T = 80$ K), during melting ($T = 100$ K) and in the fluid ($T = 120$ K) for the vacancy-dominated regime (top row), large vacancy patches (second row down), the connected network (third row down) and patches (bottom row).

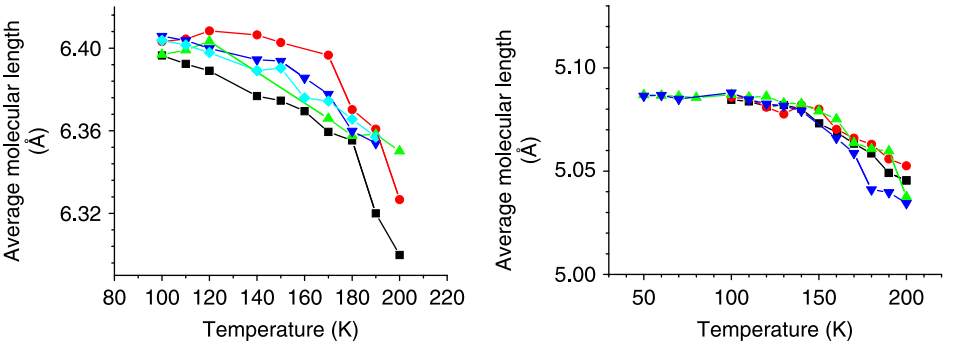

Figure 8. Average end-to-end molecular lengths as functions of temperature for C5 and C6 (left and right panels, respectively) for various densities. (Colour online).

It is clear that the RC solid and liquid coexist near melting. This effect is more pronounced for C5 than for C6, which agrees with experiment [6,7].

Both C6 and C5 show totally different flexibility. It is a consequence of different chain lengths: C6 has three dihedrals and can more easily bend than C5, which possesses only one dihedral and can be considered as rigid. Figure 8 shows the end-to-end molecule lengths for C5 and C6 over the temperature ranges studied. The comparison of both graphs clearly shows that facility of gauche defects formation (and, consequently, the change of molecular end-to-end length) is related to changes in density and temperature in C6, but not so for C5. In the case of changing density in the solid, the defects are static but in the melt they fluctuate considerably and are dynamics in nature. These data support the hypothesis that C6 is the shortest alkane whose flexibility matters for bulk phase behaviour [20]. It is also consistent with previous results showing that molecular defects were present in connected networks and were seen mostly at domain boundaries [19]. Sharp drops in the average molecular lengths observed for C5 at high temperatures correspond to molecules' desorption from the substrate: this process (as well as adsorbtion from the gas phase) may involve some flexibility of molecules; neither case is the focus of the study reported here.

4. Conclusions

The major conclusions of this work are as follows: (i) There seem to be four unique topological regimes common to both C6 and C5 systems on graphite at densities in this work – below where the UI submonolayer phase exists and open space is present in the lattice. (ii) Small vacancies are present at the highest densities followed in decreasing density by large vacancy patches, then connected networks over an intermediate density range and finally individual patches at the lowest densities studied. (iii) Based on energetics and structural information, the small vacancy regime persists down to about $\rho = 0.8$ for both systems and, based on melting temperatures, individual islands begin to form below about $\rho = 0.5$. The energetics does not show a signature of the transition from large vacancy patches to any of the lower density regimes because, at all densities below the small vacancy region, the system is driven by edge to interior ratios. (iv) In the small vacancy region, the melting temperature is sensitive to changes in density because the domains are hindered upon expansion to fill up the empty space upon melting. (v) As density decreases from the small vacancy region to support large vacancy patches, overall orientational order for the adlayer decreases in favour of a larger number of smaller domains with varying orientations. Upon melting, the empty space is not filled up: as there is minimal hindrance upon expansion, the melting temperature is insensitive to changes in density. (vi) As the system's density decreases from the vacancy patch regime to the connected network, the number of smaller domains with different orientations increases and the overall orientational order of the adlayer is completely lost. (vii) In the lowest density regime, the melting temperature again becomes sensitive to changes in average density due to finite patch-size effects and surface to interior ratios of the adsorbate islands formed. (viii) The C5 system shows that, around melting, there are dense liquid clusters coexisting with the RC solid, as seen in experiment. (ix) While on graphite, C5 may be considered as rigid but static and dynamic torsional defects are present in C6 with changing density and temperature, respectively.

Acknowledgements

Acknowledgement is made to the Donors of The American Chemical Society Petroleum Research Fund (PRF43277-B5), and the University of Missouri Research Board, for the support of this research. This material is based upon work supported in part by the Department of Energy under Award No. DE-FG02-07ER46411 (CW, LF, BK) and the California Energy Commission Contract No. 500-08-022 (CW, MWR). The authors acknowledge useful discussions with Haskell Taub, Flemming Hansen and Paul Gray. We gratefully acknowledge the generous computational resources provided by the University of Missouri Bioinformatics Consortium as well as the University of Northern Iowa Computer Science Department.

References

[1] S.M. Clarke, A. Inaba, T. Arnold, and R.K. Thomas, *Calorimetric investigation of the monolayers formed at solid–liquid interface*, J. Therm. Anal. Calorim. 57 (1999), pp. 643–651.

[2] T. Arnold, C.C. Dong, R.K. Thomas, M.A. Castro, A. Perdigon, S.M. Clarke, and A. Inaba, *The crystalline structures of the odd alkanes pentane, heptane, nonane, undecane, tridecane and pentadecane monolayers adsorbed on graphite at submonolayer coverages and from the liquid*, Phys. Chem. Chem. Phys. 4 (2002), pp. 3430–3435.

[3] B.E. Matthies, *Diffraction studies of* n*-alkane films deposited on graphite*, Ph.D. diss., University of Missouri, 1999.

[4] M.A. Castro, S.M. Clarke, A. Inaba, T. Arnold, and R.K. Thomas, *Anomalous behaviour of pentane adsorbed at the graphite/liquid interface*, Phys. Chem. Chem. Phys. 1 (1999), pp. 5203–5207.

[5] M.A. Castro, S.M. Clarke, A. Inaba, T. Arnold, and R.K. Thomas, *Solid monolayers of heptane adsorbed to graphite from its liquid*, J. Phys. Chem. Solids 60 (1999), pp. 1495–1497.

[6] F. Kruchten, K. Knorr, U.G. Volkmann, H. Taub, F.Y. Hansen, B. Matthies, and K.W. Herwig, *Ellipsometric and neutron diffraction study of pentane physisorbed on graphite*, Langmuir 21 (2005), pp. 7507–7512.

[7] J. Krim, J. Suzanne, H. Schechter, R. Wang, and H. Taub, *LEED and neutron diffraction study of hexane adsorbed on graphite in the monolayer range: Uniaxial commensurate–incommensurate transition*, Surf. Sci. 162 (1985), pp. 446–451.

[8] J.C. Newton, *The structure and phase transitions of linear chain hydrocarbons on graphite*, Ph.D. diss., University of Missouri, 1989.

[9] H. Taub, in *NATO Advanced Study Institutes, Series C: Mathematical and Physical Sciences*, G.J. Long and F. Grandjean, eds., Vol. 228, Kluwer, Dordrecht, 1988, pp. 467–497.

[10] F.Y. Hansen and H. Taub, *Melting mechanism in monolayers of flexible rod-shaped molecules*, Phys. Rev. Lett. 69 (1992), pp. 652–655.

[11] F.Y. Hansen, J.C. Newton, and H. Taub, *Molecular dynamics studies of the melting of butane and hexane monolayers adsorbed on the basal-plane surface of graphite*, J. Chem. Phys. 98 (1993), pp. 4128–4141.

[12] K.W. Herwig, Z. Wu, P. Dai, H. Taub, and F.Y. Hansen, *Quasielastic neutron scattering and molecular dynamics simulations studies of the melting transition in butane and hexane monolayers adsorbed on graphite*, J. Chem. Phys. 107 (1997), pp. 5186–5196.

[13] E. Velasco and G.H. Peters, *Effect of substrate potential strength on the melting temperature of a hexane monolayer adsorbed on graphite*, J. Chem. Phys. 102 (1995), pp. 1098–1099.

[14] G.H. Peters and D.J. Tildesley, *Molecular dynamics simulations of the melting of a hexane monolayer: Isotropic versus anisotropic force fields*, Langmuir 12 (1996), pp. 1557–1565.

[15] G.H. Peters, *The molecular dynamics simulations of the melting of a hexane bilayer*, Surf. Sci. 347 (1996), pp. 169–181.

[16] M.W. Roth, C.L. Pint, and C. Wexler, *Phase transitions in hexane monolayers physisorbed onto graphite*, Phys. Rev. B 71 (2005), pp. 155427–155439.

[17] C.L. Pint, M.W. Roth, and C. Wexler, *Behavior of hexane on graphite at near-monolayer densities: Molecular dynamics study*, Phys. Rev. B 73 (2006), pp. 85422–85431.

[18] M.J. Connolly, M.W. Roth, C. Wexler, and P.A. Gray, *Molecular dynamics simulations of hexane deposited onto graphite: An explicit–hydrogen model at $\rho=1$*, Am. J. Undergrad. Res. 6 (2007), pp. 27–32.

[19] M.J. Connolly, M.W. Roth, P.A. Gray, and C. Wexler, *Explicit hydrogen molecular dynamics simulations of hexane deposited onto graphite at various coverages*, Langmuir 24 (2008), pp. 3228–3234.

[20] L. Firlej, B. Kuchta, M.W. Roth, and C. Wexler, *Non-universality of energy scaling in simulations of intermediate and long alkanes adsorbed on graphite*, J. Comp. Theor. Chem., submitted.

[21] C. Wexler, L. Firlej, B. Kuchta, and M.W. Roth, *Melting of hexane monolayers adsorbed on graphite: The role of domains and defect formation*, Langmuir Lett. 25 (2009), pp. 6596–6598.

[22] L. Kale, R. Skeel, R. Brunner, M. Bhandarkar, A. Gursoy, N. Krawetz, J. Phillips, A. Shinozaki, K. Varadarajan, and K. Schulten, *NAMD2: Greater scalability for parallel molecular dynamics*, J. Comp. Phys. 151 (1999), pp. 283–312. Available at http://www.ks.uiuc.edu/Research/namd/.

[23] S. Jha, P.V. Coveney, and C.A. Laughton, *Forcefield validation for nucleic acid simulations: Comparing energies and dynamics of a DNA dodecamer*, J. Comp. Chem. 26 (2005), pp. 1617–1627.

[24] R.W. Benz, F. Castro-Román, D.J. Tobias, and S.H. White, *Experimental validation of molecular dynamics simulations of lipid bilayers: A new approach*, Biophys. J. 88 (2005), pp. 805–817.

[25] W.A. Steele, *The physical interaction of gases with crystalline solids. I. Gas–solid energies and properties of isolated adsorbed atoms*, Surf. Sci. 36 (1973), pp. 317–352.

[26] B.R. Brooks, R.E. Bruccoleri, B.D. Olafson, D.J. States, S. Swaminathan, and M. Karplus, *CHARMM: A program for macromolecular energy, minimization, and dynamics calculations*, J. Comp. Chem. 4 (1983), pp. 187–217. Available at http://www.charmm.org.

[27] L. Firlej, B. Kuchta, M.W. Roth, M.J. Connolly, and C. Wexler, *Structural and phase properties of tetracosane ($C_{24}H_{50}$) monolayers adsorbed on graphite: An explicit hydrogen molecular dynamics study*, Langmuir 24 (2008), pp. 12392–12397.